Turbulent Boundary Layers Over Surfaces Smoothed by Sanding

Michael P. Schultz
Naval Architecture & Ocean Engineering Department,
United States Naval Academy,
Annapolis, MD 21402

Karen A. Flack
Mechanical Engineering Department,
United States Naval Academy,
Annapolis, MD 21402

Flat-plate turbulent boundary layer measurements have been made on painted surfaces, smoothed by sanding. The measurements were conducted in a closed return water tunnel, over a momentum thickness Reynolds number (Re_θ) range of 3000 to 16,000, using a two-component laser Doppler velocimeter (LDV). The mean velocity and Reynolds stress profiles are compared with those for smooth and sandgrain rough walls. The results indicate an increase in the boundary layer thickness (δ) and the integral length scales for the unsanded, painted surface compared to a smooth wall. More significant increases in these parameters, as well as the skin-friction coefficient (C_f) were observed for the sandgrain surfaces. The sanded surfaces behave similarly to the smooth wall for these boundary layer parameters. The roughness functions (ΔU^+) for the sanded surfaces measured in this study agree within their uncertainty with previous results obtained using towing tank tests and similarity law analysis. The present results indicate that the mean profiles for all of the surfaces collapse well in velocity defect form. The Reynolds stresses also show good collapse in the overlap and outer regions of the boundary layer when normalized with the wall shear stress. [DOI: 10.1115/1.1598992]

Introduction

The importance of rough wall, turbulent boundary layers is well established. In a large number of engineering applications, from pipe flow to flow over a ship's hull, boundary layers develop over surfaces that are rough to an appreciable degree. For this reason, a significant body of research has focused on quantifying the effect of surface roughness on boundary layer structure. Numerous experimental investigations of rough wall, turbulent boundary layers have been conducted including the studies of Clauser [1], Hama [2], Ligrani and Moffat [3], Krogstad and Antonia [4–6], and others. Raupach et al. [7] provides an excellent review of much of this work. The majority of these investigations have centered on flows over simple, well-defined roughness patterns such as transverse bars, mesh screen, sandgrains, and circular rods. While use of simple roughness geometry is attractive since it is easily defined and can be parametrically altered, it is not representative of most roughness of engineering interest. A notable exception was the study of Acharya et al. [8] that documented the effect of surface roughness caused by machining, such as that observed on turbine blades.

In many cases, turbulent flows evolve over painted surfaces that have been smoothed by sanding (e.g., sailing hulls and wind and water tunnel models). In a previous study using a towing tank, Schultz [9] documented the effect of sanding on surface roughness and frictional resistance of flat plates; however, no measurements of the mean and turbulent velocity profiles were made. The purpose of the present investigation is to document the mean velocity and Reynolds stress profiles over these surfaces and compare them to smooth and sandgrain rough walls (i.e., sandpaper covered surfaces). This should provide a framework from which to address the similarities and differences observed in turbulent boundary layers on sanded, painted surfaces to those developing over smooth and sandgrain surfaces.

The mean velocity profile in the overlap and outer region for a smooth wall, turbulent boundary layer can be expressed as

$$U^+ = \frac{1}{\kappa}\ln(y^+) + B + 2\omega(y/\delta)\Pi/\kappa. \tag{1}$$

Clauser [1] argued that the primary effect of surface roughness was to cause a downward shift in the logarithmic region of the mean velocity profile for the boundary layer. For so-called "k-type" rough walls, the downward shift, ΔU^+, called the roughness function, correlates with k^+, the roughness Reynolds number, defined as the ratio of the roughness length scale, k, to the viscous length scale, ν/u_τ. The mean velocity profile in a rough wall boundary layer is, therefore, given as

$$U^+ = \frac{1}{\kappa}\ln((y+\varepsilon)^+) + B - \Delta U^+ + 2\omega((y+\varepsilon)/\delta)\Pi/\kappa. \tag{2}$$

Hama [2] showed that by evaluating Eqs. (1) and (2) at $y = y + \varepsilon = \delta$, the roughness function is found by subtracting the rough wall log-law intercept from the smooth wall intercept, B, at the same value of Re_{δ^*}. The roughness function can be expressed as

$$\Delta U^+ = \left(\sqrt{\frac{2}{C_f}}\right)_s - \left(\sqrt{\frac{2}{C_f}}\right)_R. \tag{3}$$

It should be noted that Eq. (3) is only valid provided the mean velocity profiles collapse in velocity defect form, given as, [1],

$$\frac{U_e - U}{u_\tau} = f\left(\frac{y}{\delta}\right). \tag{4}$$

Collapse of the mean defect profiles for rough and smooth walls is consistent with the turbulence similarity hypotheses of Townsend [10] and Perry and Li [11] that state that turbulence outside of the roughness sublayer (i.e., the layer of fluid immediately adjacent to the roughness) is independent of the surface condition at sufficiently high Reynolds number. A majority of the experimental evidence seems to support the universality of the defect law. Some recent research, however, indicates that surface roughness alters the velocity defect profile, [4,8], leads to a higher degree of isotropy of the Reynolds normal stresses, [4–6], and changes the Reynolds shear stress profiles in the outer region of the boundary layer, [4–6]. Another outstanding issue is the ability to characterize the roughness function (ΔU^+) for a generic surface by a physical measurement of the surface roughness (k) alone.

The goal of the present experimental investigation is to document the mean velocity and Reynolds stress profiles on painted surfaces smoothed by sanding. These are compared with profiles over smooth and sandgrain rough walls. An attempt to identify a suitable roughness scaling parameter for the roughness function

Contributed by the Fluids Engineering Division for publication in the JOURNAL OF FLUIDS ENGINEERING. Manuscript received by the Fluids Engineering Division August 19, 2002; revised manuscript received March 23, 2003. Associate Editor: M. V. Otügen.

 Copyright © 2003 by ASME

Table 1 Description and roughness statistics of the test surfaces

Specimen	R_a (μm)	R_q (μm)	R_t (μm)	R_z (μm)	Description
Smooth	NA	NA	NA	NA	Cast acrylic surface
60-grit sandpaper	126±5	160±7	983±89	921±82	60-grit commercial wet/dry sandpaper
220-grit sandpaper	30±2	38±2	275±17	251±14	220-grit commercial wet/dry sandpaper
Unsanded	9±1	12±1	76±8	71±7	Unsanded, sprayed polyamide epoxy
60-grit sanded	5±1	4±1	36±4	32±3	Sprayed polyamide epoxy sanded with 60-grit wet/dry sandpaper
120-grit sanded	4±1	3±1	26±2	23±2	Sprayed polyamide epoxy sanded with 120-grit wet/dry sandpaper

Uncertainties represent the 95% confidence precision bounds

for this particular class of surfaces is made. These results are compared with the roughness function measured indirectly for these surfaces by Schultz [9] using frictional resistance measurements on towed flat plates.

Experimental Facilities and Method

The present experiments were carried out in the closed circuit water tunnel facility at the United States Naval Academy Hydromechanics Laboratory. The test section is 40 cm by 40 cm in cross section and is 1.8 m in length, with a tunnel velocity range of 0–6.0 m/s. In the present investigation, the freestream velocity was varied between ~1.0 m/s–3.5 m/s ($\mathrm{Re}_x=1.4\times10^6-4.9\times10^6$). Flow management devices include turning vanes placed in the tunnel corners and a honeycomb flow straightener in the settling chamber. The honeycomb has 19 mm cells that are 150 mm in length. The area ratio between the settling chamber and the test section is 20:1, and the resulting freestream turbulence intensity in the test section is ~0.5%.

The test specimens were inserted into a flat-plate test fixture mounted horizontally in the tunnel. The test fixture is similar to that used by Schultz [12]. The fixture is 0.40 m in width, 1.68 m in length, and 25 mm thick. It is constructed of a high density foam core covered with carbon fiber reinforced plastic skins and was mounted horizontally in the tunnel's test section along its centerline. The leading edge of the test fixture is elliptically shaped with an 8:1 ratio of the major and minor axes. The forward most 200 mm of the plate is covered with 36-grit sandpaper to trip the developing boundary layer. The use of a strip of roughness was shown by Klebanoff and Diehl [13] to provide effective boundary layer thickening and a fairly rapid return to self-similarity. The test specimen mounts flush into the test fixture and its forward edge is located immediately downstream of the trip. The removable test specimens are fabricated from 12-mm thick cast acrylic sheet 350 mm in width and 1.32 m in length. The boundary layer profiles presented here were taken 1.35 m downstream of the leading edge of the test fixture. Profiles taken from 0.75 m to the measurement location confirmed that the flow had reached self-similarity. The trailing 150 mm of the flat plate fixture is a movable tail flap. This was set with the trailing edge up at ~5 deg in the present experiments to prevent separation at the leading edge of the plate. The physical growth of the boundary layer and the inclined tail flap created a mildly favorable pressure gradient at the measurement location. The acceleration parameter (K) varied from 7.4×10^{-8} at the lowest freestream velocity to 2.0×10^{-8} at the highest freestream velocity. The pressure gradient did not vary significantly between the test specimens.

Six test surfaces were tested in the present study (Table 1). Three served as controls. One was a smooth cast acrylic surface. The other two were sandgrain rough surfaces; one covered with 60-grit wet/dry sandpaper and the other with 220-grit wet/dry sandpaper. The remaining three test surfaces consisted of acrylic plates initially painted with several coats of marine polyamide epoxy paint manufactured by International Paint. The paint was applied with a spray gun. One surface was tested in the unsanded condition. One was wet sanded with 60-grit sandpaper. The final test surface was wet sanded with 120-grit sandpaper. All the sanding in the present experiment was carried out by hand with the aid of a sanding block using small circular motions. The surfaces were carefully cleaned with water and a soft cloth to remove grit and detritus left behind by the sanding process. Further detail of the surface preparation is given in Schultz [9]. The surface roughness profiles of the test plates were measured using a Cyber Optics laser diode point range sensor (model #PRS 40) laser profilometer system mounted to a Parker Daedal two-axis traverse with a resolution of 5 μm. The resolution of the sensor is 1 μm with a laser spot diameter of 10 μm. Data were taken over a sampling length of 50 mm and were digitized at a sampling interval of 25 μm. Ten linear profiles were taken on each of the test surfaces. No filtering of the profiles was conducted except to remove any linear trend in the trace. A description of the test surfaces along with the surface roughness statistics is given in Table 1. It should be noted that an error in the calibration used in [9] led to a systematic underestimate of the roughness height parameters. This has been remedied and the roughness height parameters given here have been verified using a second profilometer.

Velocity measurements were made using a TSI IFA550 two-component fiber-optic LDV system. The LDV used a four beam arrangement and was operated in backscatter mode. The probe volume diameter was ~90 μm, and its length was ~1.3 mm. The viscous length (ν/u_τ) varied from a minimum of 5 μm for 60-grit sandpaper at the highest Reynolds number to 24 μm for the smooth wall at the lowest Reynolds number. The diameter of the probe volume, therefore, ranged from 3.8 to 18 viscous lengths in the present study. The LDV probe was mounted on a Velmex three-axis traverse unit. The traverse allowed the position of the probe to be maintained to ±10 μm in all directions. In order to facilitate two-component near-wall measurements, the probe was tilted downwards at an angle of 4 deg to the horizontal and was rotated 45 deg about its axis. Velocity measurements were conducted in coincidence mode with 20,000 random samples per location. Doppler bursts for the two channels were required to fall within a 50 μs coincidence window or the sample was rejected.

In this study, the skin-friction coefficient, C_f, for the smooth surface was found using the Clauser chart method, [1], with log-law constants $\kappa=0.41$ and $B=5.0$. For the rough walls, C_f was obtained using a procedure based on the modified Clauser chart method given by Perry and Li [11]. To accomplish this, the wall datum offset was first determined using an iterative procedure. This involved plotting U/U_e versus $\ln[(y+\varepsilon)U_e/\nu]$ for points in the log-law region (points between $(y+\varepsilon)^+=60$ and $(y+\varepsilon)/\delta=0.2$) based on an initial guess of u_τ obtained using the total stress method detailed below. The wall datum offset was initially taken to be zero and was increased until the goodness of fit of linear regression through the points was maximized. This was

Table 2 Boundary layer parameters for the test cases

Specimen	Test Case	U_e (ms^{-1})	Re_θ	$C_f \times 10^3$ Clauser	$C_f \times 10^3$ Total Stress	δ (mm)	δ^* (mm)	θ (mm)	H	ΔU^+
Smooth	1	0.94	2950	3.44	3.32	28	3.8	2.9	1.30	—
	2	2.60	7020	2.99	3.04	26	3.2	2.5	1.27	—
	3	2.99	8080	2.92	2.82	27	3.2	2.5	1.26	—
	4	3.58	9680	2.82	2.77	26	3.2	2.5	1.26	—
60-grit sandpaper	1	0.93	3720	4.82	4.55	33	5.1	3.7	1.38	4.5
	2	2.53	10600	5.04	5.29	33	5.5	3.9	1.42	7.4
	3	3.12	13800	4.87	5.09	33	5.9	4.1	1.44	8.0
	4	3.58	16400	4.84	5.13	34	6.1	4.3	1.43	8.3
220-grit sandpaper	1	0.95	3420	3.52	3.66	33	4.7	3.5	1.36	1.3
	2	2.60	8930	3.79	3.90	29	4.3	3.2	1.34	3.9
	3	3.07	11000	3.89	3.77	30	4.5	3.3	1.36	4.8
	4	3.63	12900	3.85	3.69	30	4.6	3.4	1.36	5.2
Unsanded	1	0.93	3170	3.40	3.31	31	4.1	3.2	1.30	0.3
	2	2.50	8080	3.05	3.14	31	3.8	2.9	1.29	0.9
	3	3.11	10500	2.94	2.98	31	4.0	3.1	1.29	1.3
	4	3.59	11900	2.95	2.87	31	4.0	3.1	1.29	1.6
60-grit sanded	1	0.95	2830	3.50	3.46	27	3.8	2.9	1.31	0.2
	2	2.53	6720	3.07	2.93	27	3.2	2.5	1.27	0.2
	3	3.09	8200	2.98	2.78	28	3.2	2.5	1.27	0.4
	4	3.52	9260	2.94	2.87	27	3.2	2.5	1.26	0.5
120-grit sanded	1	1.00	2920	3.46	3.43	28	3.9	3.0	1.32	0.0
	2	2.50	7070	3.06	2.93	26	3.2	2.5	1.26	0.2
	3	3.01	9700	2.81	2.65	28	3.8	3.0	1.27	0.2
	4	3.69	11400	2.83	2.68	28	3.6	2.9	1.25	0.3

considered the proper wall datum offset. The following formula was then used to determine C_f based on the slope of the regression line, [14]:

$$C_f = 2\kappa^2 \left(\frac{d(U/U_e)}{d(\ln[(y+\varepsilon)U_e/\nu])} \right)^2. \tag{5}$$

For all the test surfaces, the total stress method was also used to verify C_f. It assumes a constant stress region equal to the wall shear stress exists in the inner layer of the boundary layer. If the viscous and turbulent stress contributions are added together, an expression for C_f may be calculated as the following evaluated at the total stress plateau in the inner layer:

$$C_f = \frac{2}{U_e^2} \left[\nu \frac{\partial U}{\partial y} - \overline{u'v'} \right]. \tag{6}$$

Uncertainty Estimates

Precision uncertainty estimates for the velocity measurements were made through repeatability tests using the procedure given by Moffat [15]. Ten replicate velocity profiles were taken on both a smooth and a rough plate. The standard error for each of the measurement quantities was then calculated for both samples. In order to estimate the 95% confidence limits for a statistic calculated from a single profile, the standard deviation was multiplied by the two-tailed t value ($t=2.262$) for nine degrees-of-freedom and $\alpha=0.05$, as given by Coleman and Steele [16]. LDV measurements are also susceptible to a variety of bias errors including angle bias, validation bias, velocity bias, and velocity gradient bias, as detailed by Edwards [17]. Angle or fringe bias is due to the fact that scattering particles passing through the measurement volume at large angles may not be measured since several fringe crossings are needed to validate a measurement. In this experiment, the fringe bias was considered insignificant, as the beams were shifted above a burst frequency representative of twice the freestream velocity, [17]. Validation bias results from filtering too close to the signal frequency and any processor biases. In general these are difficult to estimate and vary from system to system. No corrections were made to account for validation bias. Velocity bias results from the greater likelihood of high velocity particles moving through the measurement volume during a given sampling period. The present measurements were burst transit time weighted to correct for velocity bias, as given by Buchhave et al. [18]. Velocity gradient bias is due to variation in velocity across the measurement volume. The correction scheme of Durst et al. [19] was used to correct u'. The corrections to the mean velocity and the other turbulence quantities were quite small and therefore neglected. An additional bias error in the v' measurements of ~2% was caused by introduction of the w' component due to inclination of the LDV probe.

These bias estimates were combined with the precision uncertainties to calculate the overall uncertainties for the measured quantities. The resulting overall uncertainty in the mean velocity is ±1%. For the turbulence quantities $\overline{u'^2}$, $\overline{v'^2}$, and $\overline{u'v'}$, the overall uncertainties are ±2%, ±4%, and ±7%, respectively. The precision uncertainties in C_f were calculated using a series of repeatability tests, in a manner similar to that carried out for velocities. These were combined with bias estimates to calculate the overall uncertainty in C_f. The uncertainty in C_f for the smooth walls using the Clauser chart method is ±4%, and the uncertainty in C_f for the rough walls using the modified Clauser chart method was ±7%. The increased uncertainty for the rough walls resulted mainly from the extra two degrees-of-freedom in fitting the log law (ε and ΔU^+). The uncertainty in C_f using the total stress method is ±8% for both the smooth and rough walls. The uncertainties in δ, δ^*, and θ are ±7%, ±4%, and ±5%, respectively.

Results and Discussion

The experimental conditions for each of the test cases are presented in Table 2. Significant increases in the physical growth of the boundary layer were noted on the unsanded and sandgrain rough surfaces compared to the smooth wall. The average increases in δ, δ^*, and θ for the unsanded surface were 16%, 19%, and 17%, respectively. The 60-grit sandpaper showed increases of 24%, 70%, and 50%, while the 240-grit sandpaper had increases of 14%, 36%, and 27% in δ, δ^*, and θ, respectively. The increase measured in these quantities compared to the smooth wall for both of the sanded surfaces was within the experimental uncertainty. The skin-friction coefficient determined using the Clauser chart and the total stress methods showed good agreement in this investigation, as the two fell within the uncertainty for all of the test cases. The values of C_f and u_τ used in the results that follow were

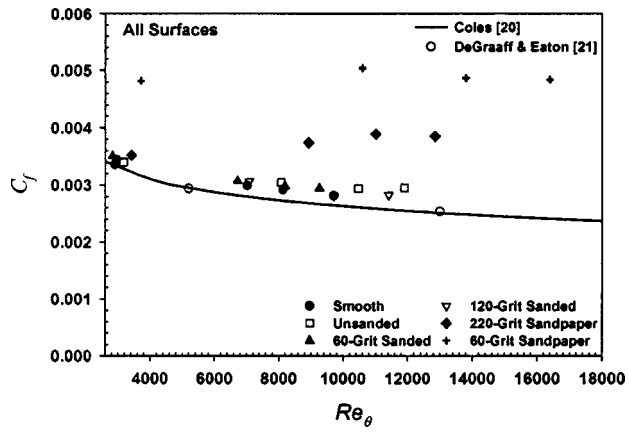

Fig. 1 Skin-friction coefficient versus momentum thickness Reynolds number. (Overall uncertainty in C_f: smooth wall, ±4%; rough wall, ±7%.)

determined using the Clauser chart method. This method was selected due to its lower overall uncertainty. Figure 1 presents C_f versus Re_θ for all the test surfaces. The smooth wall results of Coles [20] and DeGraaff and Eaton [21] are shown for comparison. The present smooth wall C_f values were systematically higher than the results of Coles and DeGraaff and Eaton by ~6% and ~4%, respectively. This may have been due to the elevated freestream turbulence intensity in the test facility and a slightly favorable pressure gradient, both of which would tend to increase C_f. It should be noted, however, that the present results agree with those of the previous investigations within the combined uncertainties of the measurements. The C_f values for the sanded and unsanded surfaces are observed to rise slightly above the smooth wall curve as Re_θ increases, however, the increases were still within the uncertainty of the measurements. The sandgrain rough surfaces both exhibited a significant increase in C_f over the entire range of Re_θ. At the highest Reynolds number, C_f was 87% higher than the smooth curve for the 60-grit sandpaper and was 43% higher for the 220-grit sandpaper.

Figure 2 shows the mean velocity profiles in wall variables for all of the test surfaces at the highest freestream velocity. The smooth profile follows the smooth wall log-law well in the overlap region. The rough surfaces also display a linear log region that is shifted by ΔU^+ below the smooth profile. As expected, a trend of increasing ΔU^+ with increasing roughness height is observed. Sanded surfaces smoother than 120-grit sanded were not tested,

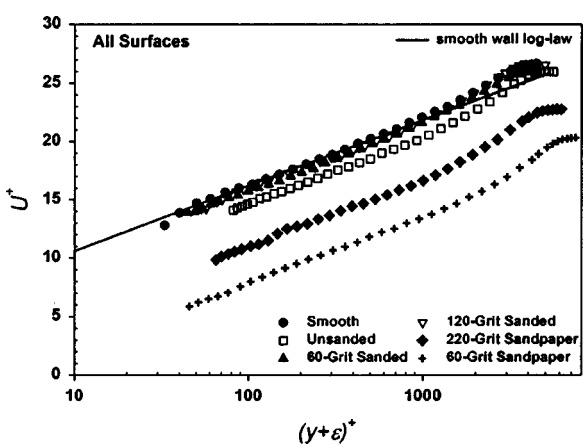

Fig. 2 Mean velocity profiles in wall coordinates for all surfaces at the highest freestream velocity. (Overall uncertainty in U^+: smooth wall, ±4%; rough wall, ±7%.)

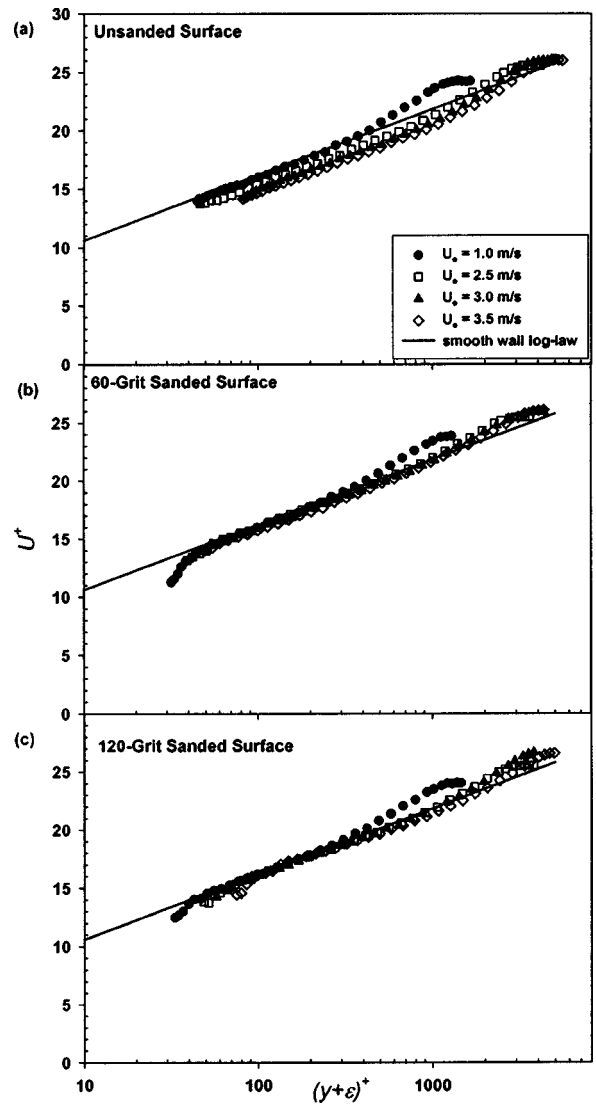

Fig. 3 Mean velocity profiles in wall coordinates for (*a*) the unsanded surface, (*b*) the 60-grit sanded surface, and (*c*) the 120-grit sanded surface. (Overall uncertainty in U^+, ±7%.)

because, as illustrated in Fig. 2, the velocity profiles were virtually collapsed with the smooth profile at this surface finish. However, in a previous study (Schultz [9]), small but significant differences in the overall frictional resistance of towed plates were observed on smoother surfaces. This implies that a roughness function may exist for surfaces sanded with finer grit sandpaper, however, they are difficult to measure using velocity profile methods. The mean velocity profiles for the sanded surfaces in wall coordinates are shown in Fig. 3. Figure 3(*a*) shows the profiles for the unsanded surface. An increase is seen in ΔU^+ with increasing unit Reynolds number, as expected. In Figs. 3(*b*) and 3(*c*), a similar trend is observed, but the changes in ΔU^+ with increasing unit Reynolds number are very small.

Figure 4 presents the roughness functions (ΔU^+ versus k^+) for all of the rough test surfaces. The Colebrook-type, [22], roughness function for naturally occurring roughness given by Grigson [23] and the Nikuradse-type, [24], roughness function for uniform sand given by Schlichting [25] are shown for comparison. The painted surfaces show good agreement ($R^2 = 0.9$) with a Colebrook-type roughness function using $k = 0.39\, R_a$. Using k based on the other roughness height parameters shown in Table 1 gave similar agreement with a Colebrook-type roughness function for these surfaces.

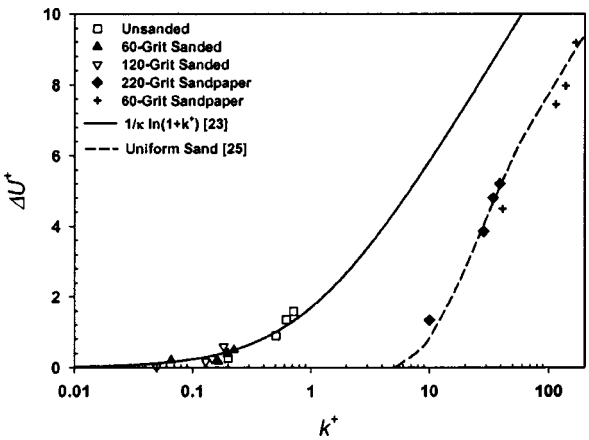

Fig. 4 Roughness functions (ΔU^+ versus k^+) for the rough specimens. (Overall uncertainty in ΔU^+, ±10% or ±0.2 whichever is greater.)

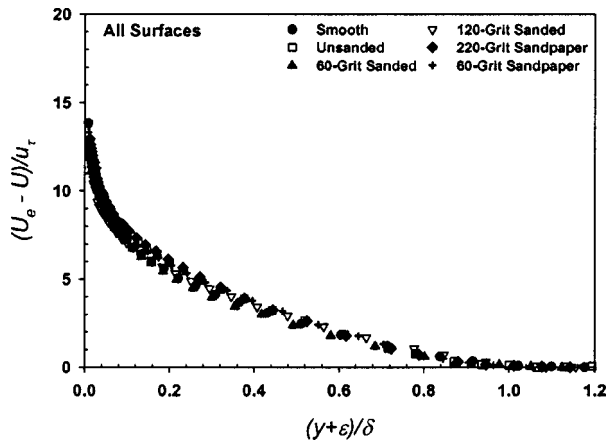

Fig. 6 Velocity defect profiles for all surfaces at the highest freestream velocity. (Overall uncertainty in $(U_e-U)/u_\tau$: smooth wall, ±5%; rough wall, ±7%.)

The sandgrain rough surfaces agree well with a Nikuradse-type roughness function with $k=0.75\,R_t$. This indicates that for these relatively simple roughness geometries a single roughness height parameter is a sufficient scaling parameter to characterize the physical nature of the surface. Acharya et al. [8] have shown that for surfaces representative of those on gas turbine blades, a texture parameter such as the root mean square deviation in the surface slope angle may be required to serve as an additional scaling parameter. It should be noted that the effect of changing the choice of k on the roughness function for a given surface is to simply shift the curve along the horizontal axis without changing its shape, since ν/u_τ and ΔU^+ are determined by the flow. Figure 5 shows the present roughness functions for the painted surfaces along with the results from similar surfaces determined by Schultz [9] using towing tank measurements and boundary layer similarity law analysis. Overall, there is good agreement between the data sets and the Colebrook-type roughness function using $k=0.39\,R_a$. These data indicate that the roughness functions determined indirectly using overall skin-friction resistance measurements and similarity law analysis can provide results that agree with those determined directly using the mean velocity profile as was argued by Granville [26].

The mean velocity profiles in defect form (Eq. (4)) for all test surfaces at the highest freestream velocity are presented in Fig. 6. The velocity defect profiles exhibit good collapse in the overlap and outer regions of the boundary layer. This supports a universal velocity defect profile for rough and smooth walls as first proposed by Clauser [1] and also lends support to the boundary layer similarity hypotheses of Townsend [10] and Perry and Li [11] that state that turbulence outside of the roughness sublayer is independent of the surface condition at sufficiently high Reynolds number. Acharya et al. [8] also noted good collapse to a universal defect profile for mesh and machined surface roughness but observed significant scatter for sand-cast surfaces.

The normalized, axial Reynolds normal stress ($\overline{u'^2}/u_\tau^2$ or equivalently $\rho\overline{u'^2}/\tau_w$) profiles for all test surfaces at the highest freestream velocity are presented in Fig. 7. Also shown for comparison are the results of the smooth wall direct numerical simulation (DNS) by Spalart [27] at $\mathrm{Re}_\theta=1410$ and the smooth and rough wall experimental results of Perry and Li [11] at $\mathrm{Re}_\theta=11{,}097$ and 7645, respectively. Good collapse of $\overline{u'^2}/u_\tau^2$ profiles is observed in both the overlap and outer regions of the boundary layer. This is in agreement with the findings of Perry and Li [11] and Krogstad and Antonia [4–6] who also observed no significant difference in the axial Reynolds normal stress profiles for smooth and rough walls outside of the inner region when they were normalized using u_τ^2. It should be noted that the present results also show good quantitative agreement with those of Perry and Li [11]. The mixed scaling ($\overline{u'^2}/u_\tau U_e$) recently proposed by DeGraaff and Eaton [21] based on a smooth wall study was also tried on the

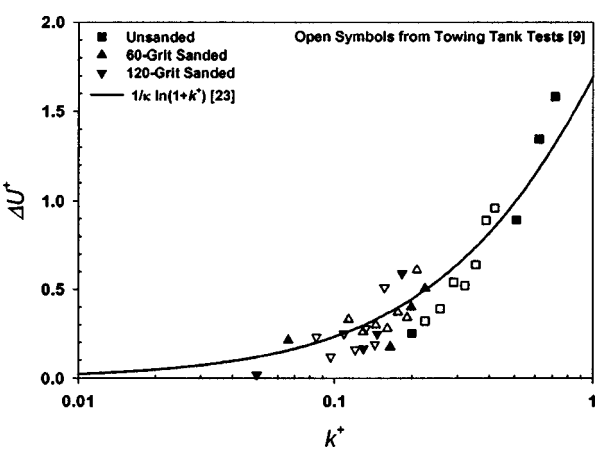

Fig. 5 Roughness functions (ΔU^+ versus k^+) for the painted surfaces. (Overall uncertainty in ΔU^+, ±0.2.)

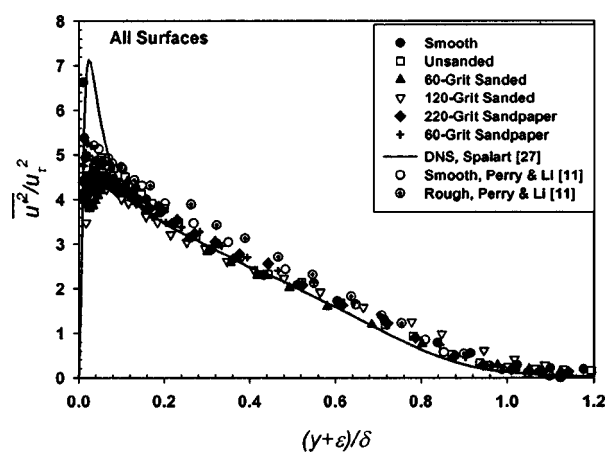

Fig. 7 Normalized axial Reynolds normal stress profiles for all surfaces at the highest freestream velocity. (Overall uncertainty in $\overline{u'^2}/u_\tau^2$: smooth wall, ±5%; rough wall, ±7%.)

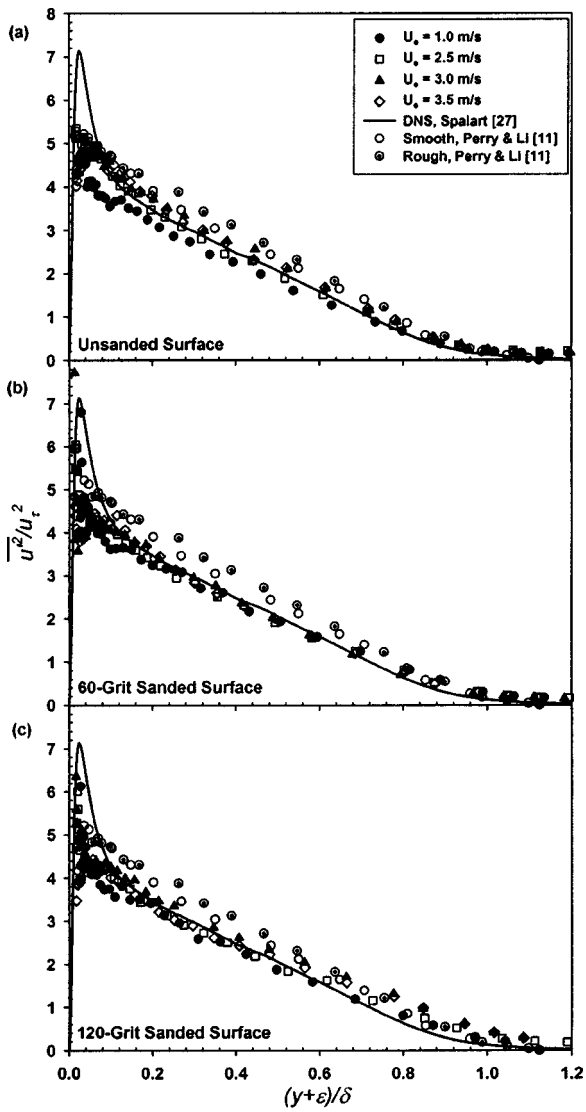

Fig. 8 Normalized axial Reynolds normal stress profiles for (*a*) the unsanded surface, (*b*) the 60-grit sanded surface, and (*c*) the 120-grit sanded surface. (Overall uncertainty in $\overline{u'^2}/u_\tau^2$, ±7%.)

present results. While it provided good collapse of the smooth wall results, it did not collapse the profiles from the different rough walls as effectively as u_τ^2. The normalized, axial Reynolds normal stress ($\overline{u'^2}/u_\tau^2$) profiles for the unsanded, 60-grit sanded, and 120-grit sanded surfaces are presented in Fig. 8. The profiles at the three highest Reynolds numbers for all of these surfaces numbers show good collapse. The lowest Reynolds number profiles are slightly below the other profiles in all cases. This is probably due to the fact that the momentum thickness Reynolds number was relatively low ($\mathrm{Re}_\theta<3200$). Coles [20] gives $\mathrm{Re}_\theta>6000$ to achieve a fully developed, equilibrium turbulent boundary layer. Again, the agreement of the present results with the smooth and rough wall results of Perry and Li [11] is within the experimental uncertainty.

The normalized, wall-normal Reynolds normal stress ($\overline{v'^2}/u_\tau^2$ or equivalently $\rho\overline{v'^2}/\tau_w$) profiles for all test surfaces at the highest freestream velocity are presented in Fig. 9. Again, the results of the smooth wall DNS by Spalart [27] and the smooth and rough wall experimental results of Perry and Li [11] are given for comparison. Good collapse of $\overline{v'^2}/u_\tau^2$ profiles is noted in both the

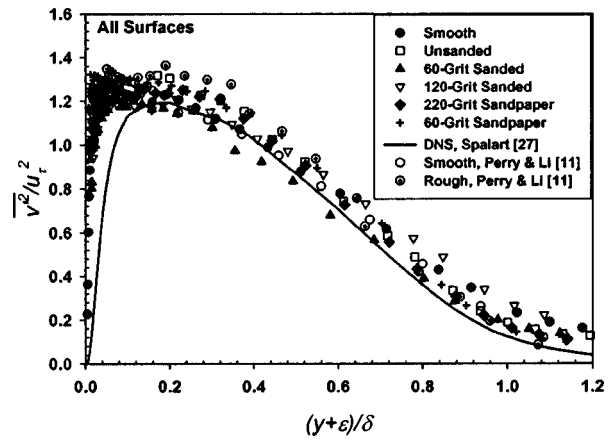

Fig. 9 Normalized wall-normal Reynolds normal stress profiles for all surfaces at the highest freestream velocity. (Overall uncertainty in $\overline{v'^2}/u_\tau^2$: smooth wall, ±6%; rough wall, ±8%.)

overlap and outer regions of the boundary layer. This is in agreement with the findings of Perry and Li [11] who also observed no significant difference in the wall-normal Reynolds normal stress profiles for smooth and rough walls outside of the near wall region when they were normalized using u_τ^2. Krogstad and Antonia [4–6] noted a large increase in $\overline{v'^2}/u_\tau^2$ well into the outer region of the boundary layer for mesh and circular rod roughness. They attributed this to an increase in the inclination angle of the large-scale structures, which tended to make the turbulence in the outer region more isotropic. Schultz [12] also observed this on flows over filamentous algae roughness but showed sandgrain roughness results collapsed well with smooth wall profiles. Further research is needed to show what surface properties are necessary to produce these changes in the boundary layer structure. It should be stated that the present results in Fig. 9 agree within their experimental uncertainty with those of Perry and Li [11]. The normalized, wall-normal Reynolds normal stress ($\overline{v'^2}/u_\tau^2$) profiles for the unsanded, 60-grit sanded, and 120-grit sanded surfaces are presented in Fig. 10. The profiles at the three highest Reynolds for all of these surface numbers show good collapse. The lowest Reynolds number profiles are slightly below the other profiles in all cases and show better agreement with the low Reynolds number DNS of Spalart [27].

The normalized, Reynolds shear stress ($-\overline{u'v'}/u_\tau^2$ or equivalently $-\rho\overline{u'v'}/\tau_w$) profiles for all surfaces at the highest freestream velocity are presented in Fig. 11. The results of the smooth wall DNS by Spalart [27], the smooth wall experimental results of DeGraaff and Eaton [21] at $\mathrm{Re}_\theta=13{,}000$, and the rough wall experimental results of Ligrani and Moffat [3] at $\mathrm{Re}_\theta=18700$ are shown for comparison. Reasonably good collapse of the $-\overline{u'v'}/u_\tau^2$ profiles is observed in both the overlap and outer regions of the boundary layer. This is in agreement with the measurements of Ligrani and Moffat [3] who also observed no significant difference between the Reynolds shear stress profiles for smooth and rough walls outside of the near wall region when they were normalized using u_τ^2. Krogstad and Antonia [4–6] noted a significant increase in $-\overline{u'v'}/u_\tau^2$ well into the outer region of the boundary layer for mesh and circular rod roughness. Schultz [12] also observed this on flows over filamentous algae roughness but showed sandgrain roughness collapsed well with smooth wall profiles. The present results in Fig. 11 agree within experimental uncertainty with those of DeGraaff and Eaton [21] and Ligrani and Moffat [3]. On the roughest surface, the 60-grit sandpaper, a local increase in $-\overline{u'v'}/u_\tau^2$ was observed in the inner region of the boundary layer. This increase persisted out to a distance of

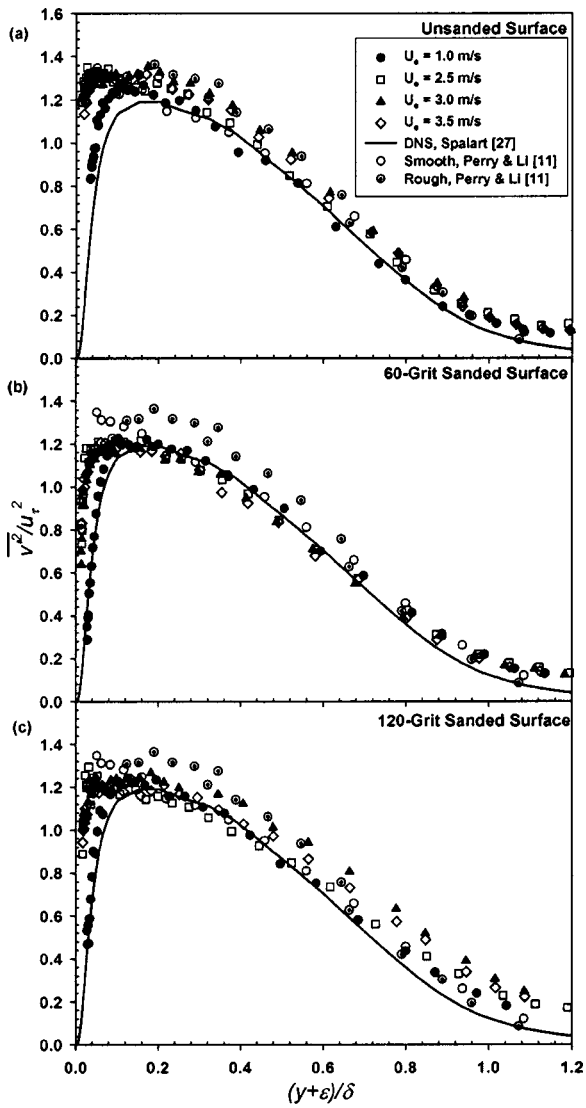

Fig. 10 Normalized wall-normal Reynolds normal stress for (*a*) the unsanded surface, (*b*) the 60-grit sanded surface, and (*c*) the 120-grit sanded surface. (Overall uncertainty in $\overline{v'^2}/u_\tau^2$, ±8%.)

$\sim 4k$ from the wall. Outside of this distance, the profile collapsed well with the others. The normalized, Reynolds shear stress ($-\overline{u'v'}/u_\tau^2$) profiles for the unsanded, 60-grit sanded, and 120-grit sanded surfaces for all freestream velocities are presented in Fig. 12. Again, agreement within the experimental uncertainty was observed between the present results and those of the previous experimental studies.

Conclusion

Comparisons of turbulent boundary layers developing over painted surfaces, smoothed by sanding with smooth and sandgrain walls have been made. An increase in the physical growth of the boundary layer was measured for the unsanded and the sandgrain roughness. A significant increase in C_f was also observed for the sandgrain surfaces. The change in these parameters for the sanded surfaces was within the experimental uncertainty. The roughness functions (ΔU^+) for the sanded surfaces measured in this study agree within their uncertainty with previous results obtained using towing tank tests and similarity law analysis. The present results show that the mean profiles for all of the surfaces collapse well in velocity defect form. Furthermore, the profiles of the normalized

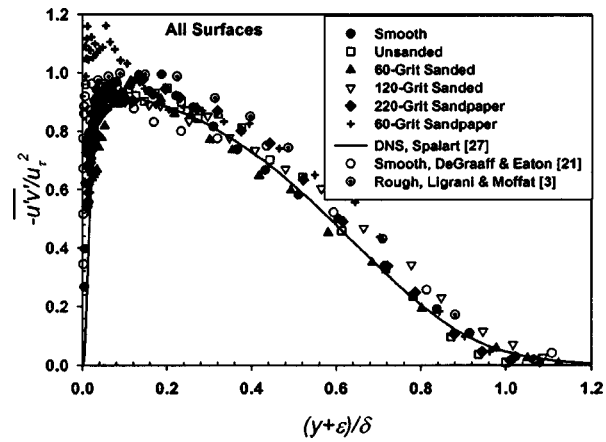

Fig. 11 Normalized Reynolds shear stress profiles for all surfaces at the highest freestream velocity. (Overall uncertainty in $-\overline{u'v'}/u_\tau^2$: smooth wall, ±8%; rough wall, ±10%.)

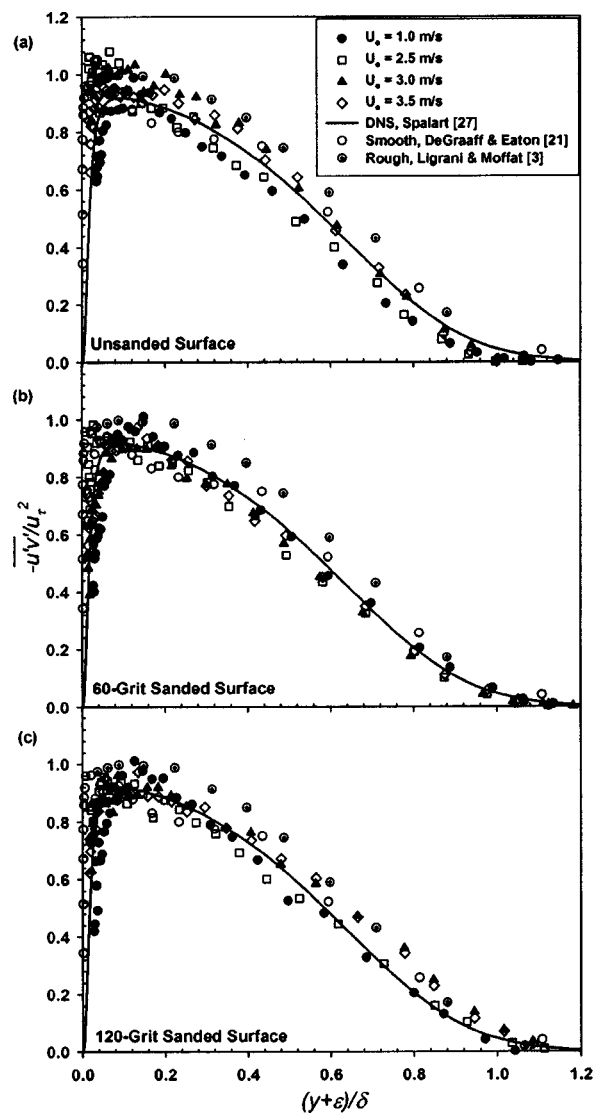

Fig. 12 Normalized Reynolds shear stress profiles for (*a*) the unsanded surface, (*b*) the 60-grit sanded surface, and (*c*) the 120-grit sanded surface. (Overall uncertainty in $-\overline{u'v'}/u_\tau^2$, ±10%.)

Reynolds stresses ($\overline{u'^2}/u_\tau^2$, $\overline{v'^2}/u_\tau^2$, and $-\overline{u'v'}/u_\tau^2$) for both the smooth and rough surfaces show agreement within experimental uncertainty in the overlap and outer regions of the boundary layer. These results lend support to the boundary layer similarity hypotheses of Townsend [10] and Perry and Li [11].

Acknowledgments

MPS would like to acknowledge the Office of Naval Research for the financial support of this research under grant #N00014-02-WR20325 administered by Dr. Steve McElvaney. Many thanks go to Mr. Don Bunker, Mr. Steve Enzinger, Mr. John Zseleczky, and the rest of the USNA Hydromechanics Lab staff for their valuable help in providing technical support for the project. We are indebted to Prof. Peter Bradshaw and Prof. Ralph Volino for many constructive comments about drafts on this manuscript. We would also like to thank Mr. Bill Beaver of the USNA Technical Support Division who constructed the flat plate test fixture and Prof. Michelle Koul for use of the laser profilometer.

Nomenclature

B = smooth wall log-law intercept, 5.0
C_f = skin-friction coefficient, $(\tau_w)/[(1/2)\rho U_e^2]$
k = arbitrary measure of roughness height
K = acceleration parameter, $(\nu/U_e^2)(dU_e/dx)$
N = number of samples in surface profile
R^2 = coefficient of determination
R_a = centerline average roughness height, $(1/N)\Sigma_{i=1}^N|y_i|$
R_q = root mean square roughness height, $\sqrt{(1/N)\Sigma_{i=1}^N y_i^2}$
R_t = maximum peak to trough height, $y_{\max}-y_{\min}$
R_z = ten point roughness height, $(1/5)\Sigma_{i=1}^5(y_{\max\, i}-y_{\min\, i})$
Re_x = Reynolds number based on distance from leading edge, $U_e x/\nu$
Re_{δ^*} = displacement thickness Reynolds number, $U_e\delta^*/\nu$
Re_θ = momentum thickness Reynolds number, $U_e\theta/\nu$
U = mean velocity in the x-direction
U_e = freestream velocity
ΔU^+ = roughness function
$\overline{u'^2}$ = streamwise mean square fluctuating velocity
$\overline{u'v'}$ = mean product of instantaneous streamwise and wall-normal fluctuating velocity
u_τ = friction velocity, $\sqrt{\tau_w/\rho}$
$\overline{v'^2}$ = wall-normal mean square fluctuating velocity
x = streamwise distance from plate leading edge
y = normal distance from the wall
δ = boundary layer thickness ($y@U=0.995U_e$)
δ^* = displacement thickness, $\int_0^\delta(1-U/U_e)dy$
ε = wall datum offset
κ = von Karman constant$=0.41$
ν = kinematic viscosity of the fluid
Π = wake parameter
θ = momentum thickness, $\int_0^\delta(U/U_e)(1-U/U_e)dy$
ρ = density of the fluid
τ_w = wall shear stress
ω = wake function

Superscripts

$+$ = inner variable (normalized with u_τ or u_τ/ν)

Subscripts

min = minimum value
max = maximum value
R = rough surface
S = smooth surface

References

[1] Clauser, F. H., 1954, "Turbulent Boundary Layers in Adverse Pressure Gradients," J. Aeronaut. Sci., **21**, pp. 91–108.
[2] Hama, F. R., 1954, "Boundary-Layer Characteristics for Rough and Smooth Surfaces," Transactions SNAME, **62**, pp. 333–351.
[3] Ligrani, P. M., and Moffat, R. J., 1986, "Structure of Transitionally Rough and Fully Rough Turbulent Boundary Layers," J. Fluid Mech., **162**, pp. 69–98.
[4] Krogstad, P.-Å., Antonia, R. A., and Browne, L. W. B., 1992, "Comparison Between Rough- and Smooth-Wall Turbulent Boundary Layers," J. Fluid Mech., **245**, pp. 599–617.
[5] Krogstad, P.-A., and Antonia, R. A., 1999, "Surface Roughness Effects in Turbulent Boundary Layers," Exp. Fluids, **27**, pp. 450–460.
[6] Antonia, R. A., and Krogstad, P.-Å., 2001, "Turbulence Structure in Boundary Layers Over Different Types of Surface Roughness," Fluid Dyn. Res., **28**, pp. 139–157.
[7] Raupach, M. R., Antonia, R. A., and Rajagopalan, S., 1991, "Rough-Wall Turbulent Boundary Layers," Appl. Mech. Rev., **44**(1), pp. 1–25.
[8] Acharya, M., Bornstein, J., and Escudier, M. P., 1986, "Turbulent Boundary Layers on Rough Surfaces," Exp. Fluids, **4**, pp. 33–47.
[9] Schultz, M. P., 2002, "The Relationship Between Frictional Resistance and Roughness for Surfaces Smoothed by Sanding," ASME J. Fluids Eng., **124**, pp. 492–499.
[10] Townsend, A. A., 1976, *The Structure of Turbulent Shear Flow*, Cambridge University Press, Cambridge, UK.
[11] Perry, A. E., and Li, J. D., 1990, "Experimental Support for the Attached-Eddy Hypothesis in Zero-Pressure Gradient Turbulent Boundary Layers," J. Fluid Mech., **218**, pp. 405–438.
[12] Schultz, M. P., 2000, "Turbulent Boundary Layers on Surfaces Covered with Filamentous Algae," ASME J. Fluids Eng., **122**, pp. 357–363.
[13] Klebanoff, P. S., and Diehl, F. W., 1951, "Some Features of Artifically Thickened Fully Developed Turbulent Boundary Layers With Zero Pressure Gradient," NACA TN 2475.
[14] Lewthwaite, J. C., Molland, A. F., and Thomas, K. W., 1985, "An Investigation into the Variation of Ship Skin Frictional Resistance with Fouling," Transactions Royal Institute of Naval Architects, **127**, pp. 269–284.
[15] Moffat, R. J., 1988, "Describing the Uncertainties in Experimental Results," Exp. Therm. Fluid Sci., **1**, pp. 3–17.
[16] Coleman, H. W., and Steele, W. G., 1995, "Engineering Application of Experimental Uncertainty Analysis," AIAA J., **33**(10), pp. 1888–1896.
[17] Edwards, R. V., 1987, "Report of the Special Panel on Statistical Particle Bias Problems in Laser Anemometry," ASME J. Fluids Eng., **109**, pp. 89–93.
[18] Buchhave, P., George, W. K., and Lumley, J. L., 1979, "The Measurement of Turbulence With the Laser-Doppler Anemometer," Annu. Rev. Fluid Mech., **11**, pp. 443–503.
[19] Durst, F., Fischer, M., Jovanovic, J., and Kikura, H., 1998, "Methods to Set Up and Investigate Low Reynolds Number, Fully Developed Turbulent Plane Channel Flows," ASME J. Fluids Eng., **120**, pp. 496–503.
[20] Coles, D., 1962, "The Turbulent Boundary Layer in a Compressible Fluid," The Rand Corp., Report R-403-PR.
[21] DeGraaff, D. B., and Eaton, J. K., 2000, "Reynolds-Number Scaling of the Flat-Plate Turbulent Boundary Layer," J. Fluid Mech., **422**, pp. 319–346.
[22] Colebrook, C. F., 1939, "Turbulent Flow in Pipes With Particular Reference to the Transition Between Smooth and Rough Pipe Laws," Journal of Civil Engineers, **11**, pp. 133–157.
[23] Grigson, C. W. B., 1992, "Drag Losses of New Ships Caused by Hull Finish," J. Ship Res., **36**, pp. 182–196.
[24] Nikuradse, J., 1933, "Laws of Flow in Rough Pipes," NACA Technical Memorandum 1292.
[25] Schlichting, H., 1979, *Boundary-Layer Theory*, 7th Ed., McGraw-Hill, New York.
[26] Granville, P. S., 1987, "Three Indirect Methods for the Drag Characterization of Arbitrarily Rough Surfaces on Flat Plates," J. Ship Res., **31**, pp. 70–77.
[27] Spalart, P. R., 1988, "Direct Simulation of a Turbulent Boundary Layer up to Re_θ=1410," J. Fluid Mech., **187**, pp. 61–98.